PHYSICAL REVIEW D **85,** 023003 (2012)

Chiral model approach to quark matter nucleation in neutron stars

Domenico Logoteta,[1] Ignazio Bombaci,[2] Constança Providência,[1] and Isaac Vidaña[1]

[1]*Centro de Física Computacional, Department of Physics, University of Coimbra, 3004-516 Coimbra, Portugal*

[2]*Dipartimento di Fisica "Enrico Fermi," Universitá di Pisa, and INFN Sezione di Pisa, Largo Bruno Pontecorvo 3, I-56127 Pisa, Italy*

(Received 29 June 2011; published 11 January 2012)

The nucleation process of quark matter in both cold and hot dense hadronic matter is investigated using a chiral approach to describe the quark phase. We use the Nambu–Jona–Lasinio and the chromo dielectric models to describe the deconfined phase and the nonlinear Walecka model for the hadronic one. The effect of hyperons on the transition phase between hadronic and quark matter is studied. The consequences of the nucleation process for neutron star physics are outlined.

DOI: 10.1103/PhysRevD.85.023003 PACS numbers: 97.60.−s, 26.60.Dd, 26.60.Kp, 97.60.Jd

I. INTRODUCTION

In the last few years, the physics of dense matter is having a growing interest due to its applications in both terrestrial (heavy ion collisions) and astrophysical (supernovae explosions and neutron stars) systems. In particular, the question of the existence of quark matter in the Universe is still an open problem. Neutron stars are among the densest objects in the Universe and, therefore, they are probably one of the best candidates to host a quark deconfined phase in their cores.

Quark matter nucleation in neutron stars has already been discussed in several previous works. Zero temperature nucleation was studied in Refs. [1–9], while in Refs. [10–15] thermal nucleation was considered. In all these papers, the MIT bag model [16] has been used for the description of the quark phase. Recently, the nucleation rate and the nucleation time have been calculated at zero and finite temperature within the same quark model [14,15]. This calculation has allowed to follow the thermal evolution of neutron stars from the young and warm proto-neutron stars to the cold ($T = 0$) and deleptonized neutron stars. The crossover temperature above which the thermal nucleation dominates quantum nucleation was calculated and the consequences of the possible quark nucleation for the physics and evolution of proto-neutron stars were discussed. It was shown that proto-hadronic stars with a gravitational mass below a critical value will survive the early stages of their evolution without decaying into a quark star. The effect of neutrino trapping on quark nucleation has been considered explicitly in Refs. [15,17].

In the present paper, we will investigate how the nucleation process depends on the quark model chosen to describe the dense quark phase. There are several chiral quark models in the literature that successfully describe the low energy properties of mesons and hadrons. In particular, we will consider two quark models which contain explicitly the chiral symmetry: the Nambu-Jona-Lasinio (NJL) model [18] and the chromo dielectric model (CDM) [19]. The NJL model (see [20] for a recent review) has been extensively used to study quark matter in β-equilibrium and quark stars [20–25]. The parameters of this model are fixed by low energy scattering data of mesons. Although the NJL model contains dynamical chiral symmetry breaking explicitly, an important symmetry of QCD, it is unable to explain confinement. This feature is maybe the main drawback of the model.

The QCD phase diagram determined with the NJL model shows that, at very high densities and low temperatures, the most favorable deconfined phase could be in a color superconducting state in which two flavors or all three quark flavors are paired [26,27]. High densities and low temperatures are the conditions which are expected to occur at the core of a neutron star some minutes after its birth. In the present paper, we do not take into account the possible formation of a color-superconducting state of dense quark matter and we use the standard version of the NJL model without superconductivity [28]. Recently, the deconfinement phase transition in proto-neutron stars within the SU(3) NJL model including 2SC color superconductivity has been discussed by the authors of Refs. [17,29].

The CDM has been used to study the static and dynamical properties of the nucleon, and describes the confinement of quarks through their interaction with a scalar field χ which represents a multigluon state and produces a density dependent constituent mass. Quark matter has been analyzed within this model in several papers [30–32].

The present work is organized as follows: first, we give a brief description of the approach used to model the hadronic phase; next we review the main features of the NJL and chromo dielectric models and present the results for quark matter nucleation in both cold and hot dense hadronic matter. Finally, the consequences of the deconfinement phase transition for neutron star physics are discussed.

II. EQUATION OF STATE

In this section, we present a brief review of the models used to build the equation of state (EOS) of stellar matter. The hadronic matter is described within

the nonlinear Walecka model (NLWM) [33] and quark matter within the NJL and the CDM models. We take $\hbar = c = 1$ in all the expressions.

A. The nonlinear Walecka model

The Lagrangian density, including the baryonic octet, in terms of the scalar σ, the vector-isoscalar ω_μ and the vector-isovector $\vec{\rho}_\mu$ meson fields reads (see *e.g.* [22,34,35])

$$\mathcal{L} = \mathcal{L}_{\rm hadrons} + \mathcal{L}_{\rm leptons} \tag{1}$$

where the hadronic contribution is

$$\mathcal{L}_{\rm hadrons} = \mathcal{L}_{\rm baryons} + \mathcal{L}_{\rm mesons} \tag{2}$$

with

$$\mathcal{L}_{\rm baryons} = \sum_B \bar{\psi}_B[\gamma^\mu D_\mu - M_B^*]\psi_B, \tag{3}$$

where

$$D_\mu = i\partial_\mu - g_{\omega B}\omega_\mu - g_{\rho B}\vec{t}_B \cdot \vec{\rho}_\mu, \tag{4}$$

and $M_B^* = M_B - g_{\sigma B}\sigma$ is the baryon effective mass. The quantity $\vec{t}_B$ designates the isospin of baryon B. The mesonic contribution reads

$$\mathcal{L}_{\rm mesons} = \mathcal{L}_\sigma + \mathcal{L}_\omega + \mathcal{L}_\rho, \tag{5}$$

with

$$\mathcal{L}_\sigma = \frac{1}{2}(\partial_\mu\sigma\partial^\mu\sigma - m_\sigma^2\sigma^2) + \frac{1}{3!}\kappa\sigma^3 + \frac{1}{4!}\lambda\sigma^4, \tag{6}$$

$$\begin{aligned}\mathcal{L}_\omega &= -\frac{1}{4}\Omega_{\mu\nu}\Omega^{\mu\nu} + \frac{1}{2}m_\omega^2\omega_\mu\omega^\mu,\\ \Omega_{\mu\nu} &= \partial_\mu\omega_\nu - \partial_\nu\omega_\mu,\end{aligned} \tag{7}$$

$$\begin{aligned}\mathcal{L}_\rho &= -\frac{1}{4}\vec{B}_{\mu\nu}\cdot\vec{B}^{\mu\nu} + \frac{1}{2}m_\rho^2\vec{\rho}_\mu\cdot\vec{\rho}^\mu,\\ \vec{B}_{\mu\nu} &= \partial_\mu\vec{\rho}_\nu - \partial_\nu\vec{\rho}_\mu - g_\rho(\vec{\rho}_\mu\times\vec{\rho}_\nu).\end{aligned} \tag{8}$$

For the lepton contribution we take

$$\mathcal{L}_{\rm leptons} = \sum_l \bar{\psi}_l(i\gamma_\mu\partial^\mu - m_l)\psi_l, \tag{9}$$

where the sum is over electrons, muons and neutrinos for matter with trapped neutrinos. In uniform matter, we get for the baryon Fermi energy $\epsilon_{\rm FB} = g_{\omega B}\omega_0 + g_{\rho B}t_{3B}\rho_{03} + \sqrt{k_{\rm FB}^2 + M_B^{*2}}$.

We will use the GM1 parametrization of NLWM due to Glendenning and Moszkowski [35,36]. The nucleon coupling constants are fitted to the bulk properties of nuclear matter. The inclusion of hyperons involves new couplings, which can be written in terms of the nucleonic ones: $g_{\sigma Y} = x_\sigma g_\sigma$, $g_{\omega Y} = x_\omega g_\omega$, $g_{\rho Y} = x_\rho g_\rho$. In this model, it is assumed that all the hyperons in the octet have the same coupling. Measured neutron star masses can be used to restrict the possible ranges of variability of the hyperon couplings [35,36]. In this work, we will consider $x_\sigma = 0.6$ and $x_\sigma = 0.7$. In addition, following Ref. [36] we will take $x_\rho = x_\sigma$, whereas the binding energy of the Λ in symmetric nuclear matter, B_Λ,

$$\left(\frac{B_\Lambda}{A}\right) = -28\ {\rm MeV} = x_\omega g_\omega\omega_0 - x_\sigma g_\sigma\sigma \tag{10}$$

is used to determine x_ω in terms of x_σ. Notice that the case with $x_\sigma = 0.6$ produces stars with a larger hyperon population (for a given stellar gravitational mass) with respect to the case $x_\sigma = 0.7$ [7,35]. In addition to these two parametrizations for hyperonic matter, we will consider the case of pure nucleonic matter (hereafter called np matter).

At zero temperature the equations of motion for the various fields can be derived using the Lagrangian of Eq. (1) and the well known Euler-Lagrange equations. At finite temperature we use the following grand canonical potential per unit volume:

$$\begin{aligned}\Omega =& \frac{1}{2}m_\sigma^2\sigma^2 + \frac{1}{3!}k\sigma^3 + \frac{1}{4!}\lambda\sigma^4 - \frac{1}{2}m_\omega^2\omega_0^2\\ &- \frac{1}{2}m_\rho^2\rho_{03}^2 - 2T\sum_{i=B}\int\frac{d^3k}{(2\pi)^3}\{\ln[1 + e^{-\beta(E_i^* - \nu_i)}]\\ &+ \ln[1 + e^{-\beta(E_i^* + \nu_i)}]\},\end{aligned} \tag{11}$$

where $\beta = 1/T$, $E_i^* = (\mathbf{k}_i^2 + M_i^{*2})^{1/2}$ and the effective chemical potential of baryon i is given by

$$\nu_i = \mu_i - g_\omega\omega_0 - \tau_{3i}g_\rho\rho_{03}. \tag{12}$$

The sum is extended to all baryons of the baryonic octet. The equations of motion are then obtained minimizing Ω with respect to the fields σ, ω_0 and ρ_{03}. The baryonic pressure and energy density are given by

$$P_B = -\Omega, \qquad \varepsilon = -P_B + \sum_{i=B}\mu_i n_i + s_B T \tag{13}$$

where n_i is the particle number density of the baryon i and s_B is the total baryonic entropy density:

$$s_B = -\left(\frac{\partial\Omega}{\partial T}\right)_{\mu_i, V}. \tag{14}$$

The total energy density and pressure are finally obtained adding the lepton contribution to P_B, ε_B and s_B.

B. The Nambu-Jona-Lasinio model

The three flavor NJL model [18] has been widely used by many authors to describe quark matter [20–25]. In this paper, we adopt the Lagrangian density of Ref. [28]:

$$\mathcal{L} = \bar{q}(i\gamma_\mu \partial^\mu - m_0)q + G\sum_{k=0}^{8}[(\bar{q}\lambda_k q)^2 + (\bar{q}i\gamma_5\lambda_k q)^2] - K[det_f(\bar{q}(1+\gamma_5)q) + det_f(\bar{q}(1-\gamma_5)q)]. \quad (15)$$

In the above expression, q denotes the three flavor quark field: $q = (u, d, s)$ and $m_0 = \mathrm{diag}(m_0^u, m_0^d, m_0^s)$ is the mass matrix. The model is not renormalizable and we use a sharp cut off Λ to treat the divergent integrals. Following [28] we take: $\Lambda = 602.3$ MeV, $G\Lambda^2 = 1.835$, $K\Lambda^2 = 12.36$, $m_0^u = 5.5$ MeV, $m_0^d = 5.5$ MeV, $m_0^s = 140.7$ MeV. These parameters have been determined by fitting the f_π (pion decay constant), m_π (pion mass), m_K (kaon mass) and $m_{\eta'}$ (η' mass) to their experimental values. Because of the interaction, the mass of the quarks in the medium (dynamical masses) are in general different from the bare masses (current masses). In the Hartree approximation, the dynamical quark masses are determined by the solution of the gap equation:

$$m_i = m_0^i - 4G < \bar{q}_i q_i > + 2K < \bar{q}_j q_j > < \bar{q}_k q_k >, \quad i \neq j \neq k. \quad (16)$$

The quark condensates $<\bar{q}_i q_i>$ at zero temperature are given by

$$< \bar{q}_i q_i > = -\frac{3}{\pi^2}\int_{k_{F_i}}^{\Lambda} dk k^2 \frac{m_i}{\sqrt{m_i^2 + k^2}}, \quad (17)$$

where $k_{F_i} = (\pi^2 n_i)^{1/3}$ is the Fermi momentum of the quark i and n_i its number density. The energy density (ε) and pressure (P) of the system are given by

$$\varepsilon = \sum_{i=u,d,s}\frac{3}{\pi^2}\int_0^{k_{F_i}} dk k^2\sqrt{m_i^2 + k^2} + B_{\mathrm{eff}}, \quad (18)$$

$$P = -\varepsilon + \sum_{i=u,d,s} n_i\sqrt{m_i^2 + k_{F_i}^2}. \quad (19)$$

In the NJL model, the bag constant is not a phenomenological input parameter, like in the MIT bag model. However, one can still define an effective bag pressure, $B_{\mathrm{eff}} = B_0 - B$, generated dynamically with origin in the spontaneous breaking of chiral symmetry, where

$$B = \sum_{i=u,d,s}\left[\frac{3}{\pi^2}\int_0^{\Lambda} dk k^2\sqrt{m_i^2 + k^2} - 2G < \bar{q}_i q_i >^2\right] + 4K < \bar{u}u > < \bar{d}d > < \bar{s}s >, \quad (20)$$

and $B_0 = B(n_u = n_d = n_s = 0)$ is introduced to ensure zero pressure at zero density and temperature.

The system of equations (16) and (17) is solved numerically for a fixed value of the baryonic density $\rho_B = (n_u + n_d + n_s)/3$ and the pressure and energy density are then calculated from Eqs. (18) and (19).

At finite temperature T, the above expressions can be generalized starting from the grand canonical potential per unit volume Ω [20]:

$$\Omega = \sum_{i=u,d,s}(\Omega_{m_i} + 2G < bar\,\bar{q}_i q_i >) - 4K < \bar{u}u > < \bar{d}d > < \bar{s}s > + B_0, \quad (21)$$

where

$$\Omega_{m_i} = \sum -\frac{3}{\pi^2}\int dk k^2[\sqrt{k^2 + m_i^2} + T\ln(1 - e^{-(\sqrt{k^2+m_i^2} - \mu_i)/T}) + T\ln(1 + e^{-(\sqrt{k^2+m_i^2} - \mu_i)/T})]. \quad (22)$$

The particle density of the quark i is given by

$$n_i = \frac{3}{\pi^2}\int dk k^2[f_i(k) - \bar{f}_i(k)], \quad (23)$$

while quark condensate becomes

$$< \bar{q}_i q_i > = \frac{3}{\pi^2}\int dk k^2 \frac{m_i}{\sqrt{m_i^2 + k^2}}[f_i(k) + \bar{f}_i(k) - 1], \quad (24)$$

being $f_i(k)$ and $\bar{f}_i(k)$ the quark and antiquark Fermi distribution functions, respectively:

$$f_i(k) = (1 + e^{(\sqrt{k^2+m_i^2} - \mu_i)/T})^{-1} \quad (25)$$

$$\bar{f}_i(k) = (1 + e^{(\sqrt{k^2+m_i^2} + \mu_i)/T})^{-1}. \quad (26)$$

The gap equations are derived minimizing Ω with respect to the constituent quark masses m_i. The expressions obtained are identical to Eqs. (16) with the quark condensate given by Eq. (24). The pressure and entropy density of the system are given by

$$P = -\Omega, \qquad s = -\left(\frac{\partial\Omega}{\partial T}\right)_{\mu_i, V}. \quad (27)$$

Finally, the energy density reads

$$\varepsilon = -P + \sum_{i=u,d,s} n_i\mu_i + sT. \quad (28)$$

C. The chromo dielectric model

The chromo dielectric model [19] is a confinement model that has been extensively used to study properties of single nucleons or to investigate quark matter in neutron stars [30,37–43] and supernovae explosions [31,44,45]. Confinement is achieved through the introduction of a scalar-isoscalar chiral singlet field χ. The Lagrangian density of the model reads

$$\mathcal{L} = i\sum_{f=u,d,s}\bar{\psi}_f\gamma^\mu\partial_\mu\psi_f + \frac{1}{2}(\partial_\mu\sigma)^2 + \frac{1}{2}(\partial_\mu\vec{\pi})^2 - U(\sigma,\vec{\pi}) + \sum_{f=u,d}\frac{g_f}{f_\pi\chi}\bar{\psi}_f(\sigma + i\gamma_5\vec{\tau}\cdot\vec{\pi})\psi_f + \frac{g_s}{\chi}\bar{\psi}_s\psi_s + \frac{1}{2}(\partial_\mu\chi)^2 - V(\chi), \quad (29)$$

where ψ_f represents the quark field of flavor f, $U(\sigma,\vec{\pi})$ is a mexican-hat potential

$$U(\sigma,\vec{\pi}) = \frac{m_\sigma^2}{8f_\pi^2}(\sigma^2 + \pi^2 - f_\pi^2), \quad (30)$$

and for χ we consider the simplest potential

$$V(\chi) = \frac{1}{2}M_\chi^2\chi^2. \quad (31)$$

The characteristic feature of the CDM is that quark masses rescale as an inverse power of the field χ and, therefore, acquire a density dependence

$$m_{u,d} = \frac{-g_{u,d}\sigma}{\chi f_\pi}, \qquad m_s = \frac{g_s}{\chi}. \quad (32)$$

In vacuum, χ vanishes thus providing confinement. The coupling constants are given by $g_{u,d} = g(f_\pi \pm \xi_3)$ and $g_s = g(2f_K - f_\pi)$, where $f_\pi = 93$ MeV and $f_K = 113$ MeV are the pion and the kaon decay constants. The other two constants ξ_3 and m_σ are fixed in such a way that: $\xi_3 = f_{K_\pm} - f_{K^0} = -0.75$ MeV and $m_\sigma = 1.2$ GeV. Following Ref. [31], for the mass M_χ of the field χ and its coupling g we take $M_\chi = 1.7$ GeV and $g = 23$ MeV, respectively. These values lead to reasonable values for the average delta-nucleon mass and for the nucleon isoscalar radius [31].

At zero temperature, the energy density in the CDM is given by

$$\varepsilon = \frac{3}{\pi^2}\sum_{i=u,d,s}\int_0^{k_{F_i}} dk k^2\sqrt{k^2 + m_i^2(\sigma,\chi)} + B_{\text{eff}}, \quad (33)$$

with

$$B_{\text{eff}} = V(\chi) + U(\sigma,\vec{\pi}=0). \quad (34)$$

In mean field approximation, the field $\vec{\pi}$ vanishes while the other two fields σ and χ are replaced by their mean values. The equations of motion are obtained by minimizing the energy density of the system. One gets

$$\frac{\partial V(\chi)}{\partial\chi} = -\sum_{i=u,d}\rho_{S_i}(k_{F_i},m_i)\frac{\sigma g_i}{f_\pi\chi^2} + \rho_{S_s}(k_{F_s},m_s)\frac{g_s}{\chi^2}, \quad (35)$$

$$\frac{\partial U(\sigma,\vec{\pi}=0)}{\partial\sigma} = \sum_{i=u,d}\rho_{S_i}(k_{F_i},m_i)\frac{g_i}{f_\pi\chi}, \quad (36)$$

with

$$\rho_{S_i}(k_{F_i},m_i) = \frac{3}{\pi^2}\int_0^{k_{F_i}} dk k^2\frac{m_i}{\sqrt{m_i^2 + k^2}}. \quad (37)$$

The inclusion of temperature in the CDM has been carried out following Ref. [30]. We can start from the grand canonical potential per unit volume Ω:

$$\Omega = \sum_{i=u,d,s} - T\frac{3}{\pi^2}\int dk k^2[\ln(1 + e^{-(\sqrt{k^2+m_i^2}-\mu_i)/T}) + \ln(1 + e^{-(\sqrt{k^2+m_i^2}+\mu_i)/T})] + B_{\text{eff}}, \quad (38)$$

where m_i and μ_i are the effective mass (defined in Eq. (32)) and the chemical potential of the quark i. Minimizing Ω with respect to σ and χ, we get the corresponding equations of motion at $T \neq 0$.

$$\left(\frac{\partial\Omega}{\partial\sigma}\right)_{\mu_i,T} = 0, \qquad \left(\frac{\partial\Omega}{\partial\chi}\right)_{\mu_i,T} = 0. \quad (39)$$

The particle densities of the three quarks are given by Eq. (23) and the pressure and energy density can be calculated using Eqs. (27) and (28).

III. PHASE EQUILIBRIUM

In the region of high density (high baryon chemical potential) and low temperature (which is the one relevant for neutron star physics) many QCD-inspired models suggest the deconfinement transition to be a first-order phase transition [46,47]). Under this assumption, the conditions for phase equilibrium are thus given by the Gibbs phase rule

$$T_H = T_Q \equiv T, \qquad P_H = P_Q \equiv P_0 \quad (40)$$

$$\mu_H(T,P_0) = \mu_Q(T,P_0) \quad (41)$$

where

$$\mu_H = \frac{\varepsilon_H + P_H - s_H T}{n_H}, \qquad \mu_Q = \frac{\varepsilon_Q + P_Q - s_Q T}{n_Q} \quad (42)$$

are the Gibbs energies per baryon (average chemical potentials) for the hadron (H) and quark (Q) phase, respectively, ε_H (ε_Q), P_H (P_Q), s_H (s_Q) and n_H (n_Q) denote, respectively, the total (*i.e.,* including leptonic contributions) energy density, total pressure, total entropy density, and baryon number density of the two phases. The pressure P_0 defines the transition point. For pressures above P_0 the hadronic phase is metastable, and the stable quark phase will appear as a result of a nucleation process.

Small localized fluctuations in the state variables of the metastable hadronic phase will give rise to virtual drops of the stable quark phase. These fluctuations are characterized

by a time scale $\nu_0^{-1} \sim 10^{-23}$ s set by the strong interaction that is responsible for the deconfinement phase transition. This time scale is many orders of magnitude smaller than the typical time scale set by weak interactions, therefore, quark flavor must be conserved during the deconfinement transition. We will refer to this form of deconfined quark matter, in which the flavor content is equal to that of the β-stable hadronic system at the same pressure and temperature, as the Q^* phase. Soon afterward a critical size drop of quark matter is formed, the weak interactions will have enough time to act, changing the quark flavor fraction of the deconfined droplet to lower its energy, and a droplet of β-stable quark matter is formed (hereafter the Q phase).

This first seed of quark matter will trigger the conversion [48–50] of the pure hadronic star to a quark star (hybrid star or strange star). Thus, pure hadronic stars with values of the central pressure larger than P_0 are metastable to the decay (conversion) to hybrid stars or to strange stars [1–8]. The mean lifetime of the metastable stellar configuration is related to the time needed to nucleate the first drop of quark matter in the stellar center and depends dramatically on the value of the stellar central pressure [1–8] and central temperature [14,15].

In order to explore the astrophysical implications of quark matter nucleation, following Refs. [1–3], we introduce the concept of *critical mass* $M_{\rm cr}$ for the hadronic star sequence.

In the case of cold and deleptonized stars, $M_{\rm cr}$ can be defined as the value of the gravitational mass of the metastable hadronic star for which the nucleation time τ takes a "reasonable small" value in comparison with typical ages of young pulsars as, *e.g.* the Crab pulsar. Thus, according to refs. [1–3] we take $M_{\rm cr}(T=0) \equiv M(\tau = 1\ {\rm yr}, T=0)$. It is worth recalling that the nucleation time is an extremely steep function of the hadronic star mass [1–3], therefore the exact value of τ chosen in the definition of $M_{\rm cr}(T=0)$ is not crucial. We have verified that changing τ from 1 yr to 10^3 s modifies $M_{\rm cr}(T=0)$ by $\sim$0.02%.

In the case of newly formed compact stars, the characteristic evolutionary time scale is the proto-hadronic star cooling time $t_{\rm cool}$, *i.e.* the time it takes the newborn star to reach a cold and deleptonized configuration. The cooling time has been evaluated to be [51] $t_{\rm cool} \sim$ a few 10^2 s. Thus, according to Refs. [14,15], we consider isoentropic stellar configurations (with an entropy per baryon $\tilde{S}$ in the range 1–$2k_B$) and define the critical mass for proto-hadronic stars as $M_{\rm cr}(\tilde{S}) \equiv M(\tau = 10^3\ {\rm s}, \tilde{S} = {\rm const})$.

Notice that pure hadronic stars with $M_{\rm HS} > M_{\rm cr}$ are very unlikely to be observed, while pure hadronic stars with $M_{\rm HS} < M_{\rm cr}$ are safe with respect to a sudden transition to quark matter. Thus $M_{\rm cr}$ plays the role of an effective maximum mass for the hadronic branch of compact stars (see discussion in Ref. [3]). While the Oppenheimer-Volkov maximum mass is determined by the overall stiffness of the equation of state for hadronic matter, the value of $M_{\rm cr}$ will depend in addition on the properties of the intermediate non β-stable Q^* phase.

IV. QUARK MATTER NUCLEATION RATES

The nucleation process of quark matter in hadronic stars can take place during different stages of their evolution [15]. This is due to the fact that nucleation can proceed both via thermal activation or quantum tunnelling (at zero or finite temperature). The core of a newborn neutron star reaches temperatures of 10–40 MeV [34,51] and, consequently, this era is dominated by the thermal nucleation regime; on the other hand a cold deleptonized neutron star can nucleate quark matter only via quantum tunnelling because the thermal nucleation time diverges in the limit of zero temperature (see [14,15] and the following discussion).

The energy barrier, which represents the difference in the free energy of the system with and without a Q^*-matter droplet, can be written as

$$U(\mathcal{R}, T) = \frac{4}{3}\pi n_{Q^*}(\mu_{Q^*} - \mu_H)\mathcal{R}^3 + 4\pi\sigma\mathcal{R}^2 \qquad (43)$$

where $\mathcal{R}$ is the radius of the droplet (supposed to be spherical), and σ is the surface tension for the surface separating the hadronic phase from the Q^* phase. The energy barrier has a maximum at the critical radius $\mathcal{R}_c = 2\sigma/[n_{Q^*}(\mu_H - \mu_{Q^*})]$. Notice that we have neglected the term associated with the curvature energy, and also the terms connected with the electrostatic energy, since they are known to introduce only small corrections [3,52]. The value of the surface tension σ for the interface separating the quark and hadronic phase is poorly known, and the values typically used in the literature range within 10–50 MeV fm^{-2} [52–54]. In the following, we assume σ to be temperature independent and we take $\sigma =$ 30 MeV fm^{-2}.

The quantum nucleation time τ_q (at zero and finite temperature) can be straightforwardly evaluated within a semiclassical approach [52,54,55]. First, one computes in the Wentzel-Kramers-Brillouin (WKB) approximation the ground state energy E_0 and the oscillation frequency ν_0 of the drop in the potential well $U(\mathcal{R}, T)$. Then, the probability of tunnelling is given by

$$p_0 = \exp\left[-\frac{A(E_0)}{\hbar}\right] \qquad (44)$$

where $A(E)$ is the action under the potential barrier, which in a relativistic framework reads

$$A(E) = \frac{2}{c}\int_{\mathcal{R}_-}^{\mathcal{R}_+}\sqrt{[2m(\mathcal{R})c^2 + E - U(\mathcal{R})][U(\mathcal{R}) - E]} \qquad (45)$$

being $\mathcal{R}_\pm$ the classical turning points and $m(\mathcal{R})$ the droplet effective mass. The quantum nucleation time is then equal to

$$\tau_q = (\nu_0 p_0 N_c)^{-1}, \tag{46}$$

with $N_c \sim 10^{48}$ being the number of nucleation centers expected in the innermost part ($r \leq R_{\rm nuc} \sim 100$ m) of the hadronic star, where pressure and temperature can be considered constant and equal to their central values.

The thermal nucleation rate can be written [56] as

$$I = \frac{\kappa}{2\pi}\Omega_0 \exp(-U(\mathcal{R}_c, T)/T) \tag{47}$$

where the statistical prefactor (see Ref. [57]), is given by

$$\Omega_0 = \frac{2}{3\sqrt{3}}\left(\frac{\sigma}{T}\right)^{3/2}\left(\frac{\mathcal{R}}{\xi_Q}\right)^4. \tag{48}$$

ξ_Q is the quark correlation length, which gives a measure of the thickness of the interface layer between the two phases (the droplet "surface thickness"). In the present calculation, we take $\xi_Q = 0.7$ fm according to the estimate given in Refs. [57,58].

For the dynamical prefactor, we have used a general expression which has been derived by Venugopalan and Vischer [59] (see also Refs. [57,60])

$$\kappa = \frac{2\sigma}{\mathcal{R}_c^3(\Delta w)^2}\left[\lambda T + 2\left(\frac{4}{3}\eta + \zeta\right)\right], \tag{49}$$

where $\Delta w = w_{Q*} - w_H$ is the difference between the enthalpy density of the two phases, λ is the thermal conductivity, and η and ζ are, respectively, the shear and bulk viscosities of hadronic matter. According to the results of Ref. [61], the dominant contribution to the prefactor κ comes from the shear viscosity η. Therefore, we take λ and ζ equal to zero, and we use for the shear viscosity the following relation [61]:

$$\eta = \frac{7.6 \times 10^{26}}{(T/\text{MeV})^2}\left(\frac{n_H}{n_0}\right)^2 \frac{\text{MeV}}{\text{fm s}}, \tag{50}$$

with $n_0 = 0.16$ fm^{-3} being the saturation density of normal nuclear matter. The thermal nucleation time τ_{th}, relative to the innermost stellar region ($V_{\rm nuc} = (4\pi/3)R_{\rm nuc}^3$) where almost constant pressure and temperature occur, can thus be written as $\tau_{th} = (V_{\rm nuc} I)^{-1}$.

V. RESULTS AND DISCUSSION

In Fig. 1, we show the Gibbs energy per baryon for the β-stable hadronic phase (continuous lines) and the Q^*-phase (dashed lines) as a function of the pressure for various parametrizations of the hadronic equation of state and the two models, NJL (left panel) and CDM (right panel), used to describe the deconfined phase. Above the phase equilibrium pressure P_0 the β-stable hadron phase is metastable, and the formation of the stable (with respect to the strong interactions) Q*-phase will occur via a nucleation process. An interesting difference exists between the NJL and the chromo dielectric model: starting with a hadronic phase made of β-stable nucleonic matter (continuous line labeled np) and next including hyperons with an increasing concentration (continuous lines labeled respectively $x_\sigma = 0.7$, and $x_\sigma = 0.6$), the transition point P_0 moves to lower values in the CDM, whereas in the NJL model the opposite behavior is observed. This ultimately can be traced back to the different numerical values and density (pressure) dependence of the dynamical strange quark mass in the two models. To elucidate this connection, we plot in Fig. 2 the masses (upper panels) and chemical potentials (lower panels) of the *u, d* and *s* quarks in the non-β-stable Q^*-phase as a function of the pressure for both models and for two different parametrizations of the hadronic phase ($x_\sigma = 0.6$, and 0.7). Here we note that the strange quark mass and chemical potential are much larger in the NJL model than in the CDM one in all range of the pressure explored, and particularly at the phase transition pressure P_0.

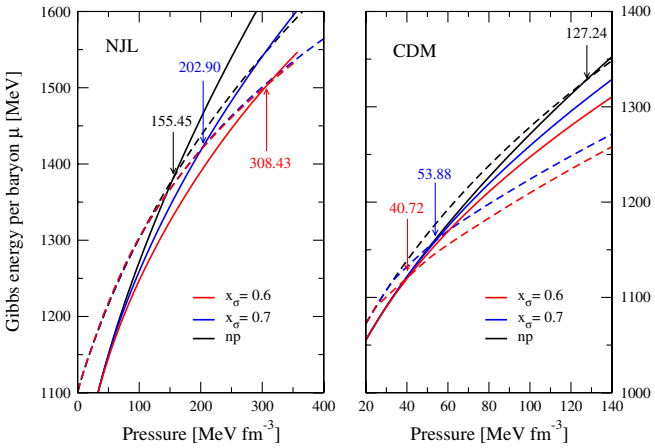

FIG. 1 (color online). Gibbs energy per baryon at zero temperature ($T = 0$) as function of the pressure for the hadronic (continuous lines) and the Q^* (dashed lines) phase. The arrows and the corresponding numbers indicate the value of the pressure P_0 at which the bulk phase transition takes place. Results for the NJL (CDM) model are shown in the left (right) panel. See text for more details.

It is important to note that a) at $P = 0$ the density of quarks *u* and *d* is not zero, $\rho_d \sim 2\rho_u$. Therefore the chemical potential is larger than the effective mass and it is larger for the *d* quarks; b) for $P < 20$–30 MeV fm^{-3} the density of s quarks is zero and the s quark chemical potential coincides with the effective s quark mass, the chemical potential decreases with the pressure because the effective mass decreases; c) above $P > 20$–30 MeV fm^{-3} the s quark density is nonzero and the chemical potential increases with the pressure. The s quark chemical potential is smaller than the *u* and *d* quark chemical potential, although the mass is larger, because the *u* and *d* quark densities are

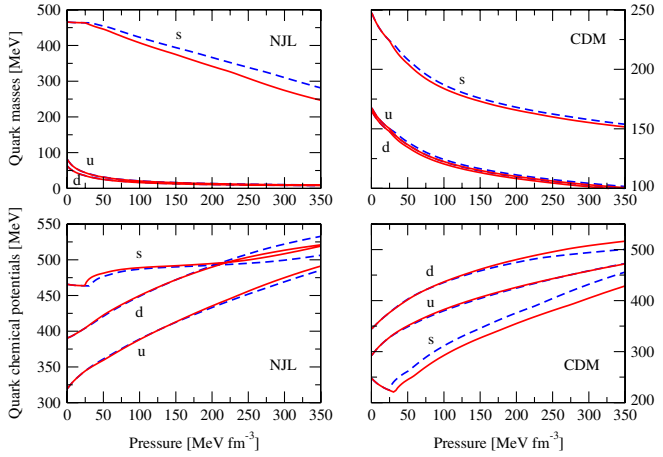

FIG. 2 (color online). Quark masses (upper panels) and chemical potentials (lower panels) in the Q^* phase at $T = 0$ using the NJL (left panels) and the CDM (right panels) models to describe the quark deconfined phase. Results for $x_\sigma = 0.6$ and $x_\sigma = 0.7$ are shown by the red continuous lines and the blue dashed ones, respectively.

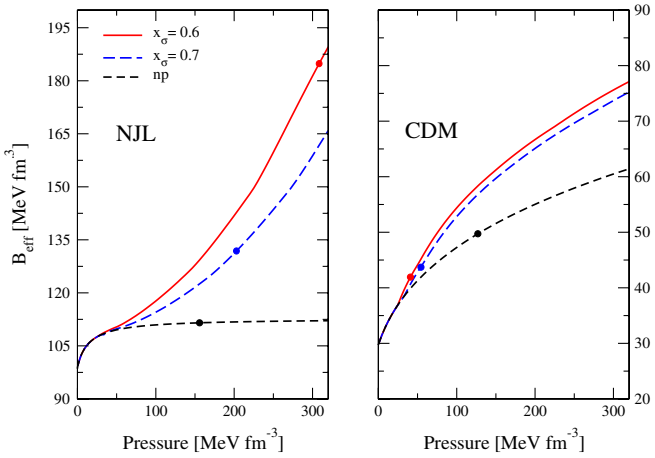

FIG. 3 (color online). Effective bag pressure at $T = 0$ for the NJL (left panel) and the CDM (right panel) models. Results for $x_\sigma = 0.6$, $x_\sigma = 0.7$ and the pure nucleonic matter case (np) are shown. The filled circle denotes the value of the effective bag pressure at the transition point P_0.

much larger. At 350 MeV fm^{-3} the fractions of quarks u, d and s are, respectively, 0.33, 0.45 and 0.22. Comparing with the NJL model, the big difference is the much larger effective mass the s quark has in NJL: the onset of the s quark occurs at the same pressure (set by the hyperon threshold in the β-stable hadronic phase) but the mass is much larger.

In order to explain the different behavior of the two chiral approaches, we observe that there are two opposite effects that define the phase transition: a smaller x_σ gives rise to a larger strangeness fraction in the hadronic phase and, therefore, to a softer hadronic EOS, shifting possible deconfinement transition point to larger densities in β-stable matter. On the other hand, the Q^* phase has the same strangeness content of the hadronic one: in the CDM model all quark masses are similar and a more symmetric uds quark matter is energetically favored, while in the NJL model the s quark mass is much larger and a larger ud quark fraction is favored. This is confirmed comparing the quark chemical potential in both models. One can see that in the NJL model an increase of the hyperonic content of the hadronic phase gives rise just to a small decrease of the strange quark chemical potential, much smaller than the one occurring in the CDM model.

It is also useful to analyze the effective bag pressure $B_{\rm eff}$ for NJL and CDM models as a function of the pressure (Fig. 3). The value of $B_{\rm eff}$ at the transition pressure P_0 is denoted with a filled circle. Coherently with the previous discussion, it is seen that for the NJL model the larger the hyperon content in the β-stable hadronic phase the larger is the value of $B_{\rm eff}$ at the transition point. The opposite behavior occurs for the CDM model. This is easily understood considering what happens in the MIT bag model for different values of the bag constant B. In this case, $B_{\rm eff}$ is a constant and the discussion carried out in this framework is more transparent. In Fig. 4, the Gibbs energy per baryon for Q^* (thin lines) and hadronic (thick lines) matter is plotted for $x_\sigma = 0.6$ and 0.7 and three values of the bag pressure B. Some conclusions are immediate: i) the larger the bag value the larger the Gibbs energy per baryon for the Q* phase therefore the transition is disfavored, ii) the smaller the x_σ value the smaller is the Gibbs energy per baryon both in the hadronic and in the Q^* phase, iii) the last effect is much larger in the Q^* phase for the smaller pressures, but becomes of the same order of magnitude in both phases for $B > 150$ MeV fm^{-3}. Taking together effect i) and iii) and observing the very different value of $B_{\rm eff}(P_0)$ in the two chiral approaches considered, we

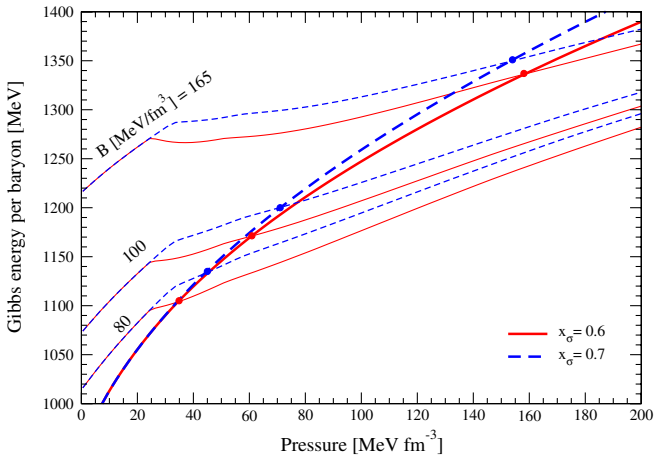

FIG. 4 (color online). Gibbs energy per baryon at $T = 0$ for the β-stable hadronic phase, with $x_\sigma = 0.6$ (continuous thick line) and $x_\sigma = 0.7$ (dashed thick line), and for the Q^* phase (thin lines). The MIT bag model has been used for the Q^* phase with a bag constant $B = 80$, 100 and 165 MeV/ fm^3.

deduce that in the NJL model the phase transition is disfavored for the smaller value of x_σ while the opposite occurs for the CDM model.

The phase equilibrium curve $P_0(T)$ between the hadron and Q^* phases is shown in Fig. 5 in the case of the NJL model (left panel) or the CDM (right panel) to describe the deconfined phase. For the hadron phase we take $x_\sigma = 0.7$ in both cases. The region of the P_0–T plane above each curve represents the deconfined Q*-phase. We have checked that in the CDM, the phase separation line moves downwards (upwards) if a hadronic EOS with a larger (smaller) strangeness content is used, *e.g.,* $x_\sigma = 0.6$ (np matter). Using the NJL model, the opposite occurs due to the reasons discussed above for the case of zero temperature phase transition.

Now we can proceed to analyze the effects of quark matter nucleation process in the core of neutron stars. We first consider quark matter nucleation in cold β-stable hadronic matter that is the typical situation in the core of a neutron star a few minutes after its birth. At this point of our discussion, we assume that quark matter nucleation has not occurred during the proto-neutron star stage (see below).

In Fig. 6 we show the gravitational mass versus central pressure for different compact star models. Hadronic star sequences are calculated using the GM1 parametrization for pure nucleonic matter (black curve), hyperonic matter with $x_\sigma = 0.7$ (blue curve) and $x_\sigma = 0.6$ (red curve). The quark star (QS) sequence is represented by the green curve. For the quark models cosidered in this paper, all QS sequences are made of hybrid stars (YS). Results in the left (right) panel are relative to the NJL (CDM) model for the quark phase. The configuration marked with an asterisk represents, in all cases, the hadronic star for which the central pressure is equal to P_0 and thus the quark matter nucleation time is $\tau = \infty$. The critical mass configuration is denoted by a full circle. The stellar conversion process [1–3] of the critical mass configuration into a final quark star with the same stellar baryonic mass (filled square) is denoted by the dashed line connecting the circle to the square. Notice that in most of the cases reported in the figure, the quark matter nucleation process will lead to the formation of a black hole (for these cases we do not plot in Fig. 6 the corresponding YS sequence). In particular, within the present values for the EOS parameters the formation of quark stars is not possible modeling the quark phase with the NJL model.

We next consider the case of new born hadronic stars (proto-hadronic stars, PHSs). In this case the quark deconfinement phase transition is likely triggered by a thermal nucleation process and it will occur in those PHSs with a gravitational mass $M > M_{\rm cr}(\tilde{S})$ [14,15]. Here we consider the case of neutrino-free matter, since it has been shown [15] that neutrino trapping does not alter substantially the outcomes of the PHS evolution.

The evolution of a PHS within this scenario is delineated in Fig. 7, where we plot the appropriate stellar equilibrium sequences in the gravitational–baryonic mass plane obtained from the CDM for the quark phase and the

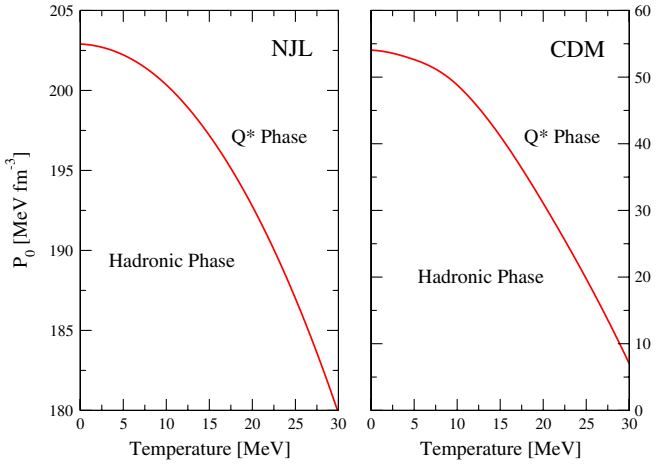

FIG. 5 (color online). Phase equilibrium curve between the β-stable hadronic phase, with $x_\sigma = 0.7$, and the Q^* phase using the NJL (left panel) and the CDM (right panel) models.

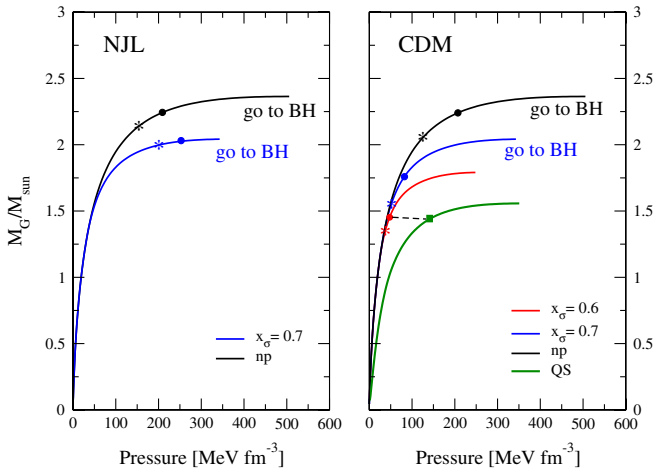

FIG. 6 (color online). Gravitational mass versus central pressure for compact stars. Hadronic star sequences are calculated using the GM1 parametrization for pure nucleonic matter (black curve), hyperonic matter with $x_\sigma = 0.7$ (blue curve) and $x_\sigma = 0.6$ (red curve). The hybrid star (YS) sequence is represented by the green curve. Results in the left (right) panel are relative to the NJL (CDM) model for the quark phase. The configuration marked with an asterisk represents in all cases the hadronic star for which the central pressure is equal to P_0 and thus the quark matter nucleation time is $\tau = \infty$. The critical mass configuration is denoted by a full circle. The conversion process of the critical mass configuration into a final quark star with the same stellar baryonic mass (filled square) is denoted by the dashed line connecting the circle to the square. In most of the cases reported in the figure, the quark matter nucleation process will lead to the formation of a black hole (go to BH). For these cases we do not plot the corresponding YS sequence.

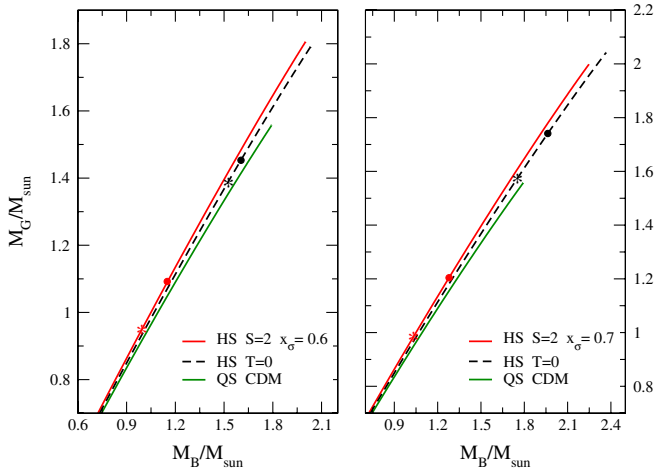

FIG. 7 (color online). Evolution of a proto-hadronic star in the gravitational–baryonic mass plane using the chromo dielectric model (CDM) to describe the quark phase and the GM1 model with $x_\sigma = 0.6$ (left panel) and $x_\sigma = 0.7$ (right panel) for the hadronic phase. The upper (red) line represents the stellar equilibrium sequence for neutrino-free proto-hadronic stars (PHS) with $\tilde{S} = 2k_B$. The (black) dashed line represents the cold the HS sequence. The asterisk and the full circle on these lines represent the stellar configuration with nucleation time $\tau = \infty$ and the critical mass configuration, respectively. The lower (green) line represent the cold YS sequence. Assuming $M_B = \text{const}$, the evolution of a PHS in this plane occurs along a vertical line.

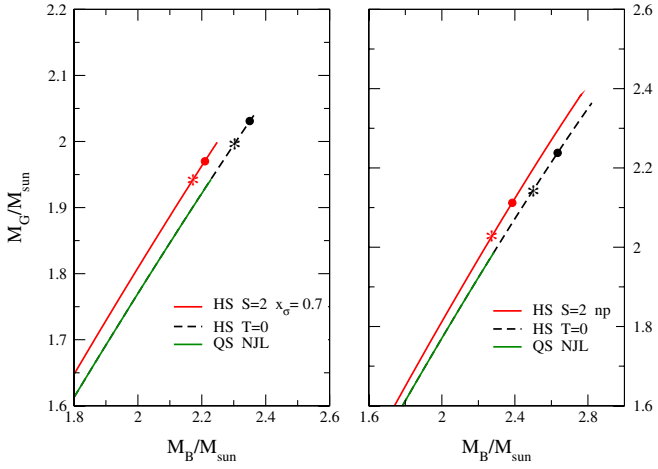

FIG. 8 (color online). Same as in the previous figure but in the case of the NJL model for the quark phase and the GM1 model for hyperonic matter with $x_\sigma = 0.7$ (left panel) and pure nucleonic (np) matter (right panel).

GM1 model in the case of hyperonic matter with $x_\sigma = 0.6$ (left panel), and $x_\sigma = 0.7$ (right panel). In particular, we plot the PHS sequence, *i.e.* isoentropic hadronic stars ($\tilde{S} = 2k_B$) and neutrino-free matter (upper line), and the cold hadronic star (HS) sequence (dashed line). The asterisk and the full circle on these lines identify, respectively, the stellar configuration with $\tau = \infty$ and the critical mass configuration. We denote as $M^{\rm PHS}_{B,\rm cr} \equiv M_{B,\rm cr}(\tilde{S} = 2k_B)$ the baryonic critical mass for the PHS sequence and as $M^{\rm HS}_{B,\rm cr} \equiv M_{B,\rm cr}(\tilde{S} = 0)$ the baryonic critical mass for the cold hadronic star sequence. The lower continuous (green) line represents the cold QS sequence having a a maximum gravitational (baryonic) mass $M^{\rm QS}_{\rm max}$ ($M^{\rm QS}_{B,\rm max}$). We assume [50]) $M_B = \text{constant}$ during these stages of the stellar evolution).[1]

Thus, according to the results in the left panel of Fig. 7, proto-hadronic stars with a baryonic mass $M_B < M^{\rm PHS}_{B,\rm cr} (= 1.16 M_\odot$ within the selected EOS parametrization) will survive Q*-matter *early nucleation* (*i.e.* nucleation within the cooling time $t_{\rm cool} \sim$ a few 10^2 s) and in the end will form stable ($\tau = \infty$) cold hadronic stars. Proto-hadronic stars with $M^{\rm PHS}_{B,\rm cr} < M_B < M^{\rm QS}_{B,\rm max}$ ($= 1.79 M_\odot$ for the present EOS) will experience early nucleation of a Q*-matter drop and will ultimately form a cold deleptonized quark star. The last possibility is for PHSs having $M_B > M^{\rm QS}_{B,\rm max}$. In this case the early nucleation of a Q*-matter drop will trigger a stellar conversion process to a cold QS configuration with $M_B > M^{\rm QS}_{B,\rm max}$, thus these PHSs will finally form black holes. A similar evolutionary path is found in the case of $x_\sigma = 0.7$ (right panel).

In Fig. 8 we plot the PHS, cold HS, and cold YS sequences in the gravitational-baryonic mass plane for the case of the NJL model for the quark phase and the GM1 model in the case of pure nucleonic matter (right panel) or hyperonic matter with $x_\sigma = 0.7$ (left panel). It is clearly seen that in the case of the NJL model it is almost impossible to populate the YS branch. Cold quark stars can be formed in the case of $x_\sigma = 0.7$ (left panel) for a very

TABLE I. Gravitational $M^{\rm HS}_{\rm cr}$ ($M^{\rm PHS}_{\rm cr}$) and baryonic $M^{\rm HS}_{B,\rm cr}$ ($M^{\rm PHS}_{B,\rm cr}$) critical mass for the cold hadronic star (proto-hadronic star) sequence. The gravitational and baryonic maximum mass for the cold hybrid star sequence are denoted, respectively, as $M^{\rm YS}_{\rm max}$ and $M^{\rm YS}_{B,\rm max}$. The values of stellar masses are in unit of the solar mass ($M_\odot = 1.989 \times 10^{33}$ g). All the results reported in the table are relative to the GM1 equation of state for the hadronic phase and the Nambu–Jona-Lasinio (NJL) model for the quark phase. The gravitational maximum mass for the cold hadronic star sequence is $M^{\rm HS}_{\rm max} = 2.042 M_\odot$ in the case of hyperonic matter with $x_\sigma = 0.7$, and $M^{\rm HS}_{\rm max} = 2.364 M_\odot$ in the case of nucleonic (np) matter.

	$M^{\rm HS}_{\rm cr}$	$M^{\rm HS}_{B,\rm cr}$	$M^{\rm PHS}_{\rm cr}$	$M^{\rm PHS}_{B,\rm cr}$	$M^{\rm YS}_{\rm max}$	$M^{\rm YS}_{B,\rm max}$
$x_\sigma = 0.7$	2.025	2.342	1.964	2.201	1.943	2.293
np	2.238	2.634	2.112	2.386	1.988	2.287

[1]Sizeable mass accretion on the proto-neutron star occurs within a time of ~0.5 s after core bounce [34,51]). During the subsequent stages, the star thus evolves with $M_B \simeq \text{const}$.

TABLE II. Same as in Table I but using the CDM for the quark phase. The gravitational maximum mass for the cold hadronic star sequence is $M^{\rm HS}_{\rm max} = 1.791 M_\odot$ in the case $x_\sigma = 0.6$, and $M^{\rm HS}_{\rm max} = 2.042 M_\odot$ in the case $x_\sigma = 0.7$.

x_σ	$M^{\rm HS}_{\rm cr}$	$M^{\rm HS}_{B,{\rm cr}}$	$M^{\rm PHS}_{\rm cr}$	$M^{\rm PHS}_{B,{\rm cr}}$	$M^{\rm YS}_{\rm max}$	$M^{\rm YS}_{B,{\rm max}}$
0.6	1.453	1.604	1.092	1.153	1.557	1.793
0.7	1.741	1.963	1.204	1.279	1.557	1.793

narrow range of baryonic stellar masses $2.20 < M_B/M_\odot < 2.23 M_\odot$.

Finally, in Tables I and II we report the values of the gravitational and baryonic critical mass for the PHS and HS sequences for the two adopted quark matter models. As it has been found in previous works [14,15], thermal effects reduce the values of the critical mass and increase the portion of the quark star branch that can populated via the stellar conversion process [1,2,50]. Notice that the maximum mass configuration of the YS sequence is insensitive, in the case of the CDM, to the value of the hyperon coupling x_σ, since in this case the threshold density for quark deconfinement is much lower than the density for the onset of hyperons.

VI. CONCLUSION

In this paper, we have studied the nucleation of quark matter in both hot and cold β-stable hadronic matter using two different models with chiral symmetry to describe the quark phase: the Nambu–Jona-Lasinio model and the CDM. For the hadronic phase we chose the GM1 parametrization of the nonlinear Walecka model and we have considered pure nucleonic matter as well as hyperonic matter with a large hyperon fraction ($x_\sigma = 0.6$), and a small hyperon fraction ($x_\sigma = 0.7$).

The nucleation process forms a short-lived transitory phase (Q^* phase) which has the same flavor content of the initial β-stable hadronic phase. This particular circumstance, together with the different pressure (density) dependence of the strange quark effective mass in the two employed quark matter models produces considerable differences on the bulk properties of the phase transition and on neutron star composition and early evolution. More precisely, we found that for the NJL model the presence of hyperons disfavor the phase transition pushing the transition point to very high densities while with the CDM the opposite behavior has been observed. In addition, we found that in the case of the NJL model it is almost impossible to populate the quark star branch and that quark matter nucleation will lead to the formation of a black hole. Thus within the NJL model for the quark phase, all compact stars are pure hadronic stars. In the case of the CDM, thermal effects reduce the value of the critical mass, and both hadronic and quark star configurations can be formed as a result of the evolution of proto-hadronic stars, depending on the value of the stellar baryonic mass.

A very recent measurement [62] of the mass of the pulsar PSR J1614-2230 makes it the most massive neutron star known to date with a mass $M = (1.97 \pm 0.04) M_\odot$. Within the EOS models employed in the present work, the compact star in PSR J1614-2230 could only be a pure HS (in the case the quark phase is described by the NJL model, Fig. 8) formed from the evolution of a PHS with initial baryonic mass $M_B < M^{\rm PHS}_{B,{\rm cr}}$ and after a long-term mass accretion ($M_{\rm accr} \sim 0.1$–$0.2 M_\odot$) from a companion star in a binary system. This long-term evolution can finally form pure hadronic star with a mass $M < M^{\rm HS}_{\rm cr}$, with $M^{\rm HS}_{\rm cr} = 2.025 M_\odot$ (case $x_\sigma = 0.7$) or $M^{\rm HS}_{\rm cr} = 2.238 M_\odot$ (case of np matter). The CDM model fails to predict such a high mass.

ACKNOWLEDGMENTS

This work has been partially supported by FEDER/FCT (Portugal) under Grant Nos. SFRH/BD/62353/2009, PTDC/FIS/113292/2009 and CERN/FP/116366/2010, by the Ministero dell'Università e della Ricerca (Italy) under the PRIN 2009 project Theory of Nuclear Structure and Nuclear Matter, and by COMPSTAR, an ESF Research Networking Programme.

[1] Z. Berezhiani, I. Bombaci, A. Drago, F. Frontera, and A. Lavagno, Nucl. Phys. B, Proc. Suppl. **113**, 268 (2002).
[2] Z. Berezhiani, I. Bombaci, A. Drago, F. Frontera, and A. Lavagno, Astrophys. J. **586**, 1250 (2003).
[3] I. Bombaci, I. Parenti, and I. Vidaña, Astrophys. J. **614**, 314 (2004).
[4] A. Drago, A. Lavagno, and G. Pagliara, Phys. Rev. D **69**, 057505 (2004).
[5] G. Lugones and I. Bombaci, Phys. Rev. D **72**, 065021 (2005).
[6] I. Bombaci, G. Lugones, and I. Vidaña, Astron. Astrophys. **462**, 1017 (2007).
[7] I. Bombaci, P. K. Panda, C. Providência, and I. Vidaña, Phys. Rev. D **77**, 083002 (2008).
[8] C. Bambi and A. Drago, Astropart. Phys. **29**, 223 (2008).
[9] A. Drago, G. Pagliara, and J. Schaffner-Bielich, J. Phys. G **35**, 014052 (2008).
[10] J. E. Horvath, O. G. Benvenuto, and H. Vucetich, Phys. Rev. D **45**, 3865 (1992).
[11] J. E. Horvath, Phys. Rev. D **49**, 5590 (1994).

[12] M. L. Olesen and J. Madsen, Phys. Rev. D **49**, 2698 (1994).
[13] H. Heiselberg, in *Strangeness and Quark Matter*, edited by G. Vassiliadis (World Scientific, Singapore, 1995), p. 338.
[14] I. Bombaci, D. Logoteta, P. K. Panda, C. Providencia, and I. Vidaña, Phys. Lett. B **680**, 448 (2009).
[15] I. Bombaci, D. Logoteta, C. Providencia, and I. Vidaña, Astron. Astrophys. **528**, A71 (2011).
[16] E. Farhi and R. L. Jaffe, Phys. Rev. D **30**, 2379 (1984).
[17] G. Lugones, T. A. S. do Carmo, A. G. Grunfeld, and N. N. Scoccola, Phys. Rev. D **81**, 085012 (2010).
[18] Y. Nambu and G. Jona-Lasinio, Phys. Rev. **122**, 345 (1961).
[19] H. J. Pirner, G. Chanfray, and O. Nachtmann, Phys. Lett. B **147**, 249 (1984).
[20] M. Buballa, Phys. Rep. **407**, 205 (2005)
[21] M. Buballa, F. Neumannb, M. Oertel, and I. Shovkovyd, Phys. Lett. B **595**, 36 (2004).
[22] D. P. Menezes and C. Providência, Phys. Rev. C **68**, 035804 (2003).
[23] M. Baldo, G. F. Burgio, P. Castorina, S. Plumari, and D. Zappala', Phys. Rev. C **75**, 035804 (2007).
[24] M. Baldo, M. Buballa, G. F. Burgio, F. Neumann, M. Oertel, and H.-J. Schulze, Phys. Lett. B **562**, 153 (2003).
[25] O. Benhar and A. Cipollone, Astron. Astrophys. **525**, L1 (2011).
[26] D. Blaschke, S. Fredriksson, H. Grigorian, A. M. Oztas, and F. Sandin, Phys. Rev. D **72**, 065020 (2005).
[27] S. B. Ruester, V. Werth, M. Buballa, I. A. Shovkovy, and D. H. Rischke, Phys. Rev. D **72**, 034004 (2005).
[28] P. Rehberg, S. P. Klevansky, and J. Hufner, Phys. Rev. C **53**, 410 (1996).
[29] G. Lugones, A. G. Grunfeld, N. N. Scoccola, and C. Villavicencio, Phys. Rev. D **80**, 045017 (2009).
[30] W. Broniowski, M. Cibej, M. Kutschera, and M. Rosina, Phys. Rev. D **41**, 285 (1990).
[31] A. Drago, U. Tambini, and M. Hjorth-Jensen, Phys. Lett. B **380**, 13 (1996).
[32] A. Drago, A. Fiolhais, and U. Tambini., Nucl. Phys. **A588**, 801 (1995).
[33] B. D. Serot and J. D. Walecka, Adv. Nucl. Phys. **16**, 1 (1986); J. Boguta and A. R. Bodmer, Nucl. Phys. **A292**, 413 (1977).
[34] M. Prakash, I. Bombaci, M. Prakash, P. J. Ellis, J. M. Lattimer, and R. Knorren, Phys. Rep. **280**, 1 (1997).
[35] N. K. Glendenning, *Compact Stars* (Springer-Verlag, New-York, 2000).
[36] N. K. Glendenning and S. Moszkowski, Phys. Rev. Lett. **67**, 2414 (1991).
[37] J. A. Mcgovern, M. C. Birse, and D. Spanos, J. Phys. G **16**, 1561 (1990).
[38] S. K. Gosh and S. C. Pathak, J. Phys. G **18**, 755 (1992).
[39] T. Neuber, M. Fiolhais, K. Goeke, and J. N. Urbano, Nucl. Phys. **A560**, 909 (1993).
[40] V. Barone and A. Drago, J. Phys. G **21**, 1317 (1995).
[41] C. Maieron, M. Baldo, G. F. Burgio, and H.-J. Shulze, Phys. Rev. D **70**, 043010 (2004).
[42] W. M. Alberico, A. Drago, and C. Ratti, Nucl. Phys. **A706**, 143 (2002).
[43] S. K. Gosh, S. C. Pathak, and P. K. Sahu, Z. Phys. A **352**, 457 (1995).
[44] A. Drago and A. Lavagno, Phys. Lett. B **511**, 229 (2001).
[45] A. Drago and E. Tambini, J. Phys. G **25**, 971 (1999).
[46] Z. Fodor and S. D. Katz; Prog. Theor. Phys. Suppl. **153**, 86 (2004).
[47] S. D. H. Hsu and M. Schwetz, Phys. Lett. B **432**, 203 (1998).
[48] A. V. Olinto, Phys. Lett. B **192**, 71 (1987).
[49] H. Heiselberg, G. Baym, and C. J. Pethick, Nucl. Phys. B, Proc. Suppl. **24**, 144 (1991).
[50] I. Bombaci and B. Datta, Astrophys. J. **530**, L69 (2000).
[51] A. Burrow and J. M. Lattimer, Astrophys. J. **307**, 178 (1986).
[52] K. Iida and K. Sato, Phys. Rev. C **58**, 2538 (1998).
[53] H. Heiselberg, C. J. Pethick, and E. F. Staubo, Phys. Rev. Lett. **70**, 1355 (1993).
[54] K. Iida and K. Sato, Prog. Theor. Phys. **98**, 277 (1997).
[55] I. M. Lifshitz and Y. Kagan, Sov. Phys. JETP **35**, 206 (1972).
[56] J. S. Langer and L. A. Turski, Phys. Rev. A **8**, 3230 (1973).
[57] L. Csernai and J. I. Kapusta, Phys. Rev. D **46**, 1379 (1992).
[58] H. Heiselberg, in *Strangeness and Quark matter*, edited by G. Vassiliadis (World Scientific, Singapore, 1995), p. 338.
[59] R. Venugopalan and A. P. Vischer, Phys. Rev. E **49**, 5849 (1994).
[60] L. Csernai, J. I. Kapusta, and E. Osnes, Phys. Rev. D **67**, 045003 (2003).
[61] P. Danielewicz, Phys. Lett. B **146**, 168 (1984).
[62] P. B. Demorest, T. Pennucci, S. M. Ransom, H. S. E. Roberts, and J. W. T. Hessel, Nature (London) **467**, 1081 (2010).